



FDSRN: Fractal Deep Spiking Neural Network for Breast Cancer Detection Using Mammogram Images

Sachin Urabinahatti^{1*} D Jayadevappa² Mahendra Shivalli Jogigowda³

¹*Department of Electronics & Instrumentation Engineering JSSATE, Bangalore (Affiliated to Visvesvaraya Technological University, Karnataka)*
Department of AI & ML, BMS Institute of Technology & Management, Bengaluru, 560 119, Karnataka, India
²*Department of Electronics & Communication Engineering, Dr. H N National College of Engineering, Bangalore (Affiliated to Visvesvaraya Technological University, Karnataka) Jayanagar Bangalore – 560070, Karnataka, India*
³*Department of Medical Electronics Engineering RIT, Bangalore MSR Nagar, MSRIT Post, Bengaluru – 560 060, Karnataka, India*
 * Corresponding author's Email: sachinau@bmsit.in

Abstract: Breast cancer identification stands as a pivotal field in medical research and technology, highly focused on early identification and diagnosis of abnormalities within breast tissue. Early detection significantly enhances treatment outcomes and improves patient survival rates. By recognizing the critical significance of breast cancer identification, an innovative model known as Fractal Deep Spiking Neural Network (FDSRN) has been introduced. In this model, the mammogram images are initially chosen as input for the pre-processed phase. The preprocessing of mammogram images is accomplished by utilizing a wiener filter. After pre-processing, cancer region segmentation is implemented by utilizing U-NeXt. Then, image augmentation, such as random erasing, shifting and rotation is performed. After accomplishing image augmentation, feature extraction is applied to extract features like Gradient Binary Patterns (GBP), Binary Robust Independent Elementary Features (BRIEF) and Gray level co-occurrence matrix (GLCM). Lastly, breast cancer identification is conducted by utilizing developed FDSRN, which is the incorporation of FractalNet and Deep Spiking Neural Network (DSNN). The FDSRN employed for breast cancer detection has shown outstanding performance, achieving an accuracy of 90.205%, sensitivity of 90.710%, and specificity of 90.943%. The MIAS and DDSM datasets are used for the experimentation.

Keywords: Breast cancer detection, Mammogram images, FractalNet, Deep spiking neural network (DSNN), U-NeXt.

1. Introduction

Cancer manifests as a genetic disorder, which characterized by the acceleration of mutations that support the collection of cells exhibiting progressively aggressive traits. While the mainstream of these mutations is specific to each cancer cell, approximately 1% of cancer cases emerge from identifiable hereditary cancer syndromes, where a particular genetic mutation is present in all cells of the body. Despite their rare characteristics, these inherited syndromes hold significant biological importance [1]. Among the myriad forms of cancer,

it stands as a leading cause of morbidity and mortality in women globally [2]. The term “cancer” encompasses over a hundred variations of the disease [3]. Presently, cancer ranks as a primary cause of death worldwide, indicating a substantial rise in mortality rates, largely due to the aging population. This escalating cancer paves the way for early detection, precise tumor characterization to guide treatment decisions, and the development of effective preventative measures. Targeted therapies aimed at halting the progression of pre-cancerous cells toward malignancy offer promising avenues to address the formidable challenges associated with late-stage cancer treatment. Tumors exhibit significant

diversity in cellular characteristics, proliferation rates, genetic mutations, and responses to treatment. Understanding the molecular and cellular mechanisms underlying this tumor heterogeneity remains a crucial focus in cancer biology. Central questions revolve around whether distinct cancer subtypes originate from unique cellular sources, the contribution of genetic mutations to tumor behavior, and the relationship between the cell of origin and cancer stem cells [4]. Additionally, exploring the influence of the tumor microenvironment on tumor heterogeneity is an emerging area of interest in cancer research.

Breast cancer stands as the leading cause of cancer-related deaths among women globally [5]. It is the most prevalent malignancy affecting women, with a quarter of cases exhibiting a latent and insidious nature, characterized by slow growth and early metastasis [6]. Predominantly a postmenopausal disease, over three-quarters of breast tumors are hormone-responsive, with their progression influenced by a combination of hormonal, environmental, and genetic factors [7]. In 2018, the International Agency for Research on Cancer (IARC) of the World Health Organization (WHO) declared 17.1 million cases of breast cancer worldwide, and this number will double by 2025. Despite this being primarily a disease affecting women, breast cancer is the second deadliest malignancy, following lung cancer [5]. Breast tissue comprises connective tissue, ducts, and lobules, with cancer spreading via blood and lymphatic vessels. Metastasis involves the diffusion of cancer cells from their initial location to other areas of the body. Initially confined to the ducts or lobules, breast cancer often presents with no symptoms and has a low probability of spreading. However, over time, these tumors may progress, infiltrating surrounding breast tissue and potentially spreading to nearby lymph nodes or distant organs. The primary cause of death from breast cancer in women is widespread metastases. Early detection through routine screening significantly improves treatment outcomes and increases the likelihood of survival [8]. Additionally, advances in targeted therapies tailored to specific breast cancer subtypes have revolutionized treatment approaches, offering more personalized and effective interventions. Furthermore, ongoing research into immunotherapy and combination treatments holds promise for enhancing treatment responses and prolonging survival rates in breast cancer patients.

Early recognition of cancer is crucial for successful treatment, stimulating the development of imaging techniques aimed at enhancing the timely identification of breast cancer. Ultrasonography (US),

magnetic resonance imaging (MRI), and Mammography are the imaging methods utilized for the detection purpose. Among these, mammography stands out for its relative affordability, simplicity, speed, and widespread use in screening for early breast cancer detection. By capturing images of the breast, mammography can detect subtle changes that may escape manual examination. Utilizing reduced-energy X-rays, mammography generates images that aid in identifying the presence or absence of breast cancer [9]. It serves as a primary tool for identifying four major signs of breast cancer: Mass, Micro calcification, Architectural distortion, and Bilateral asymmetry [10]. However, manual analysis of mammogram images is prone to errors. Automating the detection and categorization of microcalcifications using a Computer-Aided Diagnosis (CAD) system could significantly improve accuracy [11]. Deep learning (DL) methods or techniques are being extensively utilized in medical imaging to create automated CAD systems. DL is renowned for its effectiveness in detecting and categorizing medical images, enabling direct extraction of significant hierarchical features ranging from low to high levels from mammogram images. DL techniques can additionally assist in interpreting mammogram images by offering quantitative measurements of tumor characteristics, such as size, shape, and texture. This makes DL the most reliable method in medical imaging for breast cancer diagnosis [5]. Some of the DL techniques commonly used for breast cancer recognition using mammogram images are Recurrent Neural Networks (RNNs), Transfer Learning, Ensemble Learning, Generative Adversarial Networks (GANs) and Convolutional Neural Networks (CNNs).

An effective model named FDSRN for breast cancer recognition by employing mammogram images is developed in this paper. The process begins the process with the pre-processing of input mammogram images utilizing the Wiener filter. Then, cancer region segmentation is implemented on the processed image using U-NeXt. After that, image augmentation, such as rotation, random erasing and shifting is performed. After performing image augmentation, the feature extraction process is accomplished to extract features like BRIEF, GBP and GLCM. At last, breast cancer is detected using devised FDSRN, which is the integrated form of DSNN and FractalNet.

The significant contribution of this paper is presented below.

- An effective model called FDSRN is devised for performing breast cancer recognition using mammogram images.

- The devised FDSRN is developed by integrating FractalNet and DSNN.

This paper contains various sections and the content involved in the section is arranged as follows: Sections 2 and 3 describe the recent work analyses with respect to this area and detailed description of devised FDSRN, respectively. Section 4 enumerates the results and evaluation and section 5 enumerates the future implementation and conclusion of this work.

2. Motivation

Breast cancer detection helps in identifying individuals at higher risk, enabling personalized preventive measures and lifestyle modifications. This proactive approach not only enhances individual health but also reduces the burden on healthcare systems by curbing the need for extensive treatments for advanced-stage cancer. By analyzing the traditional methods and importance of breast cancer detection, an innovative method named FDSRN is devised for breast cancer recognition by utilizing mammogram images.

2.1 Literature survey

Al-Fahaidy, F.A., *et al.* [2] devised Machine Learning (ML) for recognizing breast cancer by utilizing mammogram images. This approach improved the diagnostic performance by enhancing reliability through the extraction of features from digital mammograms. However, this model was unsuccessful in expanding the size of the Mammographic Image Analysis Society (MIAS) dataset using augmentation. Avci, H. and Karakaya, J., [9] introduced ML to detect breast cancer. Although this model proved effective in identifying breast lesions and differentiating between benign and malignant cases, it failed to utilize the data in light of breast cancer type and phenotype information. Rahman, H., *et al.* [5] proposed a Deep Convolutional Neural Network (DCNN) for identifying breast cancer. This method achieved efficiency in detecting and classifying malignant breast masses, producing satisfactory results and reducing computation time. However, it struggled with early-stage cancer detection due to a lack of diverse datasets covering various age intervals in breast cancer research. Ibrokhimov, B. and Kang, J.Y., [12] developed a breast cancer detection model named Two-stage deep learning (DL) method. Even though the model achieved near-optimal recognition precision on labelled test data, it was unable to develop improved standalone classifiers through experimentation with different network architectures.

Dehghan Rouzi, M., *et al.* [13] developed a Consensus-adaptive weighting (CAW) method to perform breast cancer identification. Although the model possesses the timely diagnosis and potential for increased precision, it was unsuccessful in interpreting the Digital Database for Screening Mammography (DDSM) datasets and INbreast. Elkorany, A.S. and Elsharkawy, Z.F. [8], devised a hybrid technique comprising CNNs, Term Variance (TV), and Multiclass Support Vector Machine (MSVM). The model mitigated distortion if the network becomes deeper and more complex. However, it only achieved a low-performance rate. Nagalakshmi, T., [14] proposed Ensemble-Net for recognizing breast cancer. Although the developed model achieved better precision compared to existing categorization and classical segmentation models, it was unable to focus on extracting additional features for breast tumor categorization. Almalki, Y.E., [15] designed the three-step method for detecting breast cancer. This method achieved the computerized breast cancer identification diagnostic performance. However, it failed to extend the module into a mobile application for remote access, linking patients directly with radiologists.

2.2 Major challenges

The traditional method utilized to perform breast cancer recognition by using mammogram images faces several challenges and issues. They are listed below.

- The ML model designed in [2] for breast cancer identification and diagnosis from mammography images achieved higher accuracy. However, it failed to utilize a larger size dataset for the experimentation.
- The model proposed in [5] successfully detected and classified mammograms, providing more precise results and improved visual outcomes. However, it failed to integrate other networks, such as DCNN networks like AlexNet and the VGG architecture, for early-stage cancer detection.
- In [12], a two-stage DL method was developed for breast cancer recognition. While the model improved its accuracy, it struggled to manage misclassified intra-class scores.

3. Proposed FDSRN for breast cancer detection

Breast cancer ranks higher among the most prevalent cancers worldwide, significantly impacting women's health and potentially leading to mortality.

Recent research reveals alarming statistics, indicating that approximately one in every eight women in the USA and one in every ten women in Europe are infected by breast cancer. Therefore, the critical issue lies in devising a rapid and efficient diagnostic approach. By addressing these challenges, a potent model named FDSRN is devised for performing the recognition of breast cancer. Initially, the input mammogram image is acquired from the database [16] and it is forwarded to the preprocessing phase in order to eliminate the noises present in the image using the Wiener filter [17]. Then, cancer region segmentation is performed using U-NeXt [18]. After that, image augmentation is executed and it consists of rotation, shifting and random erasing. Then, feature extraction takes place to extract the features like BRIEF [19], GBP [20] and GLCM [21]. At last, breast cancer identification is accomplished by using FDSRN, where the layers are modified. FDSRN is the combination of FractalNet [22] and DSNN [23]. The block diagram of the devised FDSRN method for detecting breast cancer using mammogram images is illustrated in Fig. 1.

The notation list of this article is provided in Table 1.

3.1 Image acquisition

The mammogram images acquired from the designed dataset [16] are chosen for whole processing and it is mathematically expressed as,

$$S = \{S_1, S_2, \dots, S_\alpha, \dots, S_\beta\} \quad (1)$$

Here, S_α is utilized as input to perform the whole breast cancer detection process.

3.2 Pre-processing using wiener filter

Pre-processing aims to improve mammogram image quality by preparing them for further processing. This is achieved by minimizing or removing unnecessary and irrelevant elements in the background of the images. The input mammogram image is preprocessed using a wiener filter [17]. This process facilitates the most accurate estimation of the initial image by ensuring a minimal Mean Square Error (MSE) between the original and the estimated image. Besides, the Wiener filter effectively handles both noise and degradation functions. In the degradation model, the mathematical representation of the discrepancy is mathematically presented as,

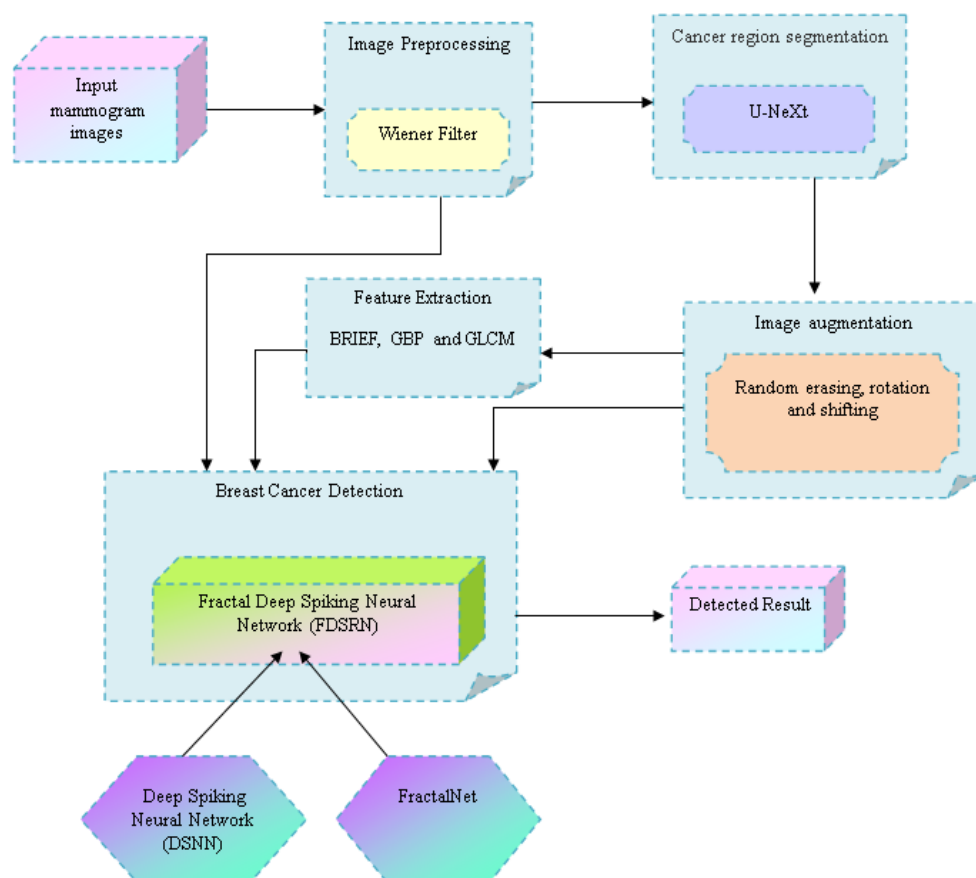


Figure. 1 Block diagram of proposed FDSRN for breast cancer detection using mammogram images

Table 1. Notation list

Notation	Definition
S	Input mammogram dataset
β	Number of images
S_α	α^{th} number of input mammogram image
$m(s_\alpha)$	Discrepancy between the input image s_α and estimated image s_α^*
P_α	Pre-processed image
W_{tc}	Transpose convolution operation
F	Output obtained from the feature map
*	Transpose convolution
s_c	Parameter of the c^{th} filter
$N_{scale}(f_c, s_c)$	Multiplication of each channel between scalar s_c and the feature map f_c
C_α	Output of U-NeXt
S_{a1}	Outcome of random erasing
S_{a2}	new pixel position after performing the rotation process
ω	angle
S_{a3}	output of shifting
A_α	combination of overall augmentation technique
τ	test
m	Patch size
$p(g_d, h_d)$	selected location pairs on a set of binary tests
p	dimensional bit string
y	function involved in GBP
T	gradients with integer
(k, l)	position of the pixel
TF	textual feature image
E_1	BRIEF feature
E_2	GBP feature
e_1	output of area
e_2	convex area output
e_3	Equivalent diameter
H and I	small diameter and large diameter of an oval
e_4	outcome of the eccentricity feature
e_6	outcome of the solidity feature
$i(t, u)$	element present in GLCM matrix
g_n	count of different gray scale
e_7	contrast feature
e_8	homogeneity feature
F_α	feature vector
D_3	spiking residual layer output
D_2	fractal-spiking residual layer output
D_1	FractalNet model output
A	FC layer
.	concatenation
r	total number of feature vector
G	weight of the input
U_1, U_2, o_1 and o_2	weight and bias of two convolutional layer
B	input from ReLU layer
D_α	input for spiking residual model
W_δ	true positive cancer instances
W_ω	true negative cancer instances
V_ω	false negative cancer instances
V_δ	false positive cancer instances

$$m(s_\alpha) = s_\alpha - s_\alpha^* \quad (2) \quad \text{The pre-processed image obtained through this phase is represented as } P_\alpha.$$

3.3 Cancer region segmentation using U-NeXt

Cancer region segmentation refers to the process of identifying and delineating areas within images that contain cancerous tissues or tumors. This segmentation is crucial in medical analysis and healing planning, as it helps clinicians to concentrate and quantify the progression of cancerous cells. Here, U-NeXt [18] is utilized to carry out cancer region segmentation. U-NeXt helps to capture subtle details and variations in medical images, making it better suited for accurately delineating cancerous regions. Additionally, U-NeXt optimizes the flow of information within the network, potentially leading to faster convergence during training and more efficient inference during segmentation tasks.

3.3.1. Architecture of U-NeXt

The U-NeXt contains an attention up-sampling block and a Skip Spatial Pyramid Pooling (SSPP) block. The input fed through U-NeXt is P_α .

A) Skip spatial pyramid pooling block

The pyramid pooling block [18] excels in gathering feature information across various scales, enhancing pixel-level detail for more effective segmentation. By aggregating context information from diverse regions, it boosts the model's capacity to capture global features. This integration of multi-scale context improves the network's ability to comprehend the broader context of the image, thus improving segmentation accuracy.

B) Attention up-sampling block

The mechanism involved in attention up-sampling [18] is similar to human selective visual attention mechanisms. Its objective is to highlight crucial facts relevant to the present task objectives from a vast array of accessible data. The attention up-sampling block primarily centers on assessing the significance of each feature channel as it undergoes the up-sampling process. It achieves this without introducing additional spatial dimensions by leveraging network loss. Subsequently, the mechanism enhances pertinent features while diminishing the influence of less relevant ones, thereby optimizing the network's performance for the task. The expressions involved in attention up-sampling block are,

$$W_{tc}: P_\alpha \rightarrow F, \quad (3)$$

The number of channels involved in feature maps remains unchanged and it is expressed as,

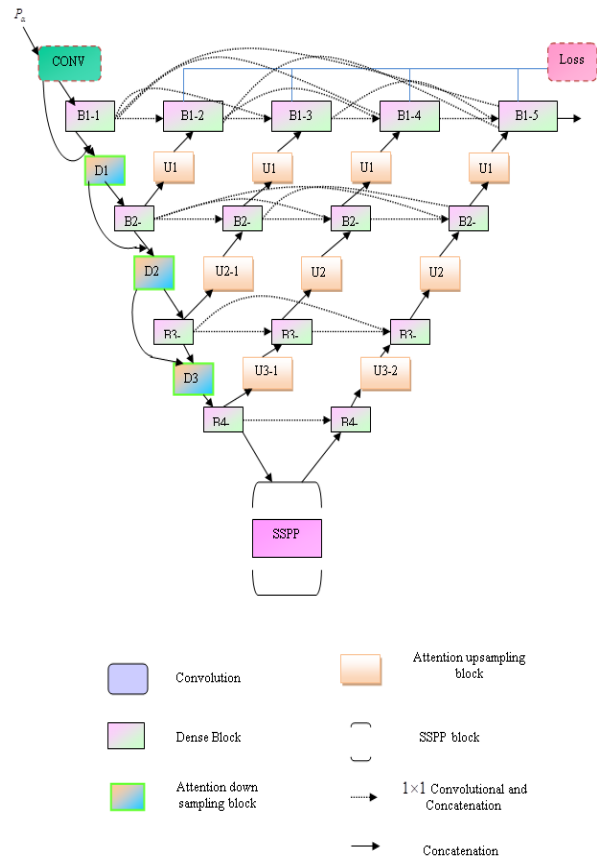


Figure. 2 Architecture of U-NeXt

$$f_c = s_c^F * P_\alpha = \sum_{j=1}^C (s_c^j)^F * w^j \quad (4)$$

$s_c = [s_c^1, s_c^2, \dots, s_c^C]$ and $P_\alpha = [w^1, w^2, \dots, w^C]$, the output denotes $F = [f_1, f_2, \dots, f_c]$. The final output S_c obtained by this layer is presented as,

$$C_\alpha = N_{scale}(f_c, s_c) = s_c * f_c \quad (5)$$

P_α is chosen as input for the segmentation process using U-NeXt and C_α is obtained as output. Fig. 2 represents the architecture diagram of U-NeXt.

3.4 Image augmentation

Image augmentation refers to the process of artificially enhancing the diversity of a dataset for training the models. Image augmentation [24] helps to overcome the limitations posed by a scarcity of data samples, especially in datasets comprised of images. The image augmentation methods, such as rotation, random erasing and shifting are utilized. C_α is the input used for image augmentation.

A) Random Erasing

Random erasing [24] is a technique used in image augmentation. It involves randomly selecting a

rectangular region within an image and replacing the pixel values in that region with random noise or a constant value. S_{a1} represents the outcome obtained by performing random erasing.

B) Rotation

The rotation [24] process involves rotating the image around an axis, either clockwise or counterclockwise, by angles ranging from 1 to 359 degrees. Rotation is applied to images by incrementally adjusting their orientation by a specified angle degree. It is mathematically expressed as,

$$S_{a2} = \begin{bmatrix} \cos \omega & -\sin \omega \\ \sin \omega & \cos \omega \end{bmatrix} \cdot \begin{bmatrix} a \\ b \end{bmatrix} \quad (6)$$

C) Shifting

Shifting [24] refers to the process of moving the pixels of an image along a specified direction (usually horizontally or vertically) by a certain distance. This movement creates a translated version of the original image, simulating variations in the position or viewpoint of the objects within the scene. S_{a3} denotes the output of the shifting augmentation technique. The overall expression for image augmentation can be expressed as,

$$A_{\alpha} = \{S_{a1}, S_{a2}, S_{a3}\} \quad (7)$$

3.5 Feature extraction

Feature extraction refers to the process of converting raw input images into meaningful features that effectively denote the underlying characteristics or patterns of the image. It also helps to lessen the dimensionality of the data while extracting the important information. The feature extraction techniques utilized in this model are BRIEF, GBP and GLCM

3.5.1. BRIEF

BRIEF [19] is a feature descriptor, which is significantly used in computer vision and image processing for tasks such as image matching, object recognition, and stereo vision. It operates by extracting binary descriptors from image patches, which are small regions within an image. The expression for BRIEF is mentioned below.

$$E_1 = \sum_{1 \leq d \leq p} 2^{d-1} \tau(m; g_d, h_d) \quad (8)$$

Here, d ranges from 1 to p .

3.5.2. GBP

GBP [20] is a type of textual operation, which is generally used in background subtraction, textual classification and face acknowledgement. The GBP method characterizes each pixel on the basis of relative intensity estimations of its neighboring pixels. It achieves estimation of neighboring pixels by quantifying the relative gradients in various directions of the pixel. It is mathematically presented as,

$$E_2 = y(\|T_1(k, l)\| - \|T_4(k, l)\|) + \dots + \sum_{m=1}^4 y(T_m(k, l)) 2^{7-m} \quad (9)$$

Here, T ranging from 0 to 2^7 .

Features such as BRIEF and GBP are performed on C_{α} to produce textual feature images. It is expressed as,

$$TF = \{E_1, E_2\} \quad (10)$$

3.5.3. GLCM

The GLCM [20] encapsulates precise information regarding the spatial distribution of gray levels within an image. It derives texture properties from images and serves as a statistical tool in image analysis. The GLCM features, like convex area, area, eccentricity, equivalent diameter, solidity, contrast, energy and homogeneity are used.

A) Area

Area [25] refers to the number of pixels present in a region.

B) Convex area

Convex area [25] refers to the number of pixels present in a convex image. This property applies exclusively to 2-D input label matrices.

C) Equivalent diameter

Equivalent diameter [25] represents the diameter of a circle that has the same area as the specified region. e_3 is mathematically denoted as,

$$e_3 = \sqrt{\frac{4 * \text{area}}{\pi}} \quad (11)$$

D) Eccentricity

Eccentricity [25] is defined as the ratio of the foci and major axis of the ellipse. This feature is only applicable for label matrices with 2-D input. The expression for eccentricity [26] can be presented as,

$$e_4 = \sqrt{1 - \frac{H^2}{I^2}} \tag{12}$$

e_4 denotes the outcome of the eccentricity feature.

E) Solidity

Solidity [25] represents the proportion of pixels in the convex hull that also belong to the specified region. It is computed as the ratio of the region's area to the area of its convex. Solidity is mathematically denoted as,

$$e_5 = \frac{e_1}{e_2} \tag{13}$$

F) Energy

Energy [27] refers to the aggregate of the GLCM squared components. The range of energy values lies between the values 0 to 1. The equation for energy is presented as,

$$e_6 = \sum_{t,u} i^2(t,u) \tag{14}$$

G) Contrast

Contrast [27] refers to the intensity difference between the pixel and its neighbors. e_7 can be mathematically expressed as,

$$e_7 = \sum_t^{g_n} \sum_u^{g_n} (t - u)^2 i(t,u) \tag{15}$$

H) Homogeneity

Homogeneity [27] refers to the likeness of GLCM within each Region of Interest (ROI) to the distribution of entities within the GLCM. Homogeneity ranges between 0 and 1. The equation for homogeneity is represented as,

$$e_8 = \sum_{t,u} \frac{i(t,u)}{1+(t,u)} \tag{16}$$

The GLCM features, such as convex area, area, eccentricity, energy, solidity, homogeneity, contrast and equivalent diameter are applied on TF to produce F_α . It is mathematically presented as,

$$F_\alpha = \{e_1, e_2, e_3, \dots, e_8\} \tag{17}$$

3.6 Breast cancer detection using FDSRN

Breast cancer detection refers to the process of identifying the existence of breast cancer in individuals. The devised FDSRN is utilized to perform breast cancer detection, which is a combination of FractalNet [22] and DSNN [23]. The FDSRN model is promising for breast cancer detection due to their ability to extract complex features from medical images, classify patterns with high accuracy, operate in real time, and potentially adapt to individual patient data for personalized diagnostics. This offers high reliability, robustness, and adaptability for the detection model. Fig. 3 represents the systematic view of the proposed FDSRN.

The devised FDSRN comprises three layers namely the FractalNet model, the Fractal-Spiking Residual layer and the Spiking Residual layer. B_α is fed as input into the FractalNet model, such that $B_\alpha \in \{P_\alpha, S_\alpha\}$ produces an outcome D_1 . Then, this outcome and extracted features F_α is utilized as input for the fractal-spiking residual layer, where fusion and regression processes are performed. The output D_2 produced from the fractal-spiking residual layer and P_α serves as input for the spiking residual layer to produce output as D_3 .

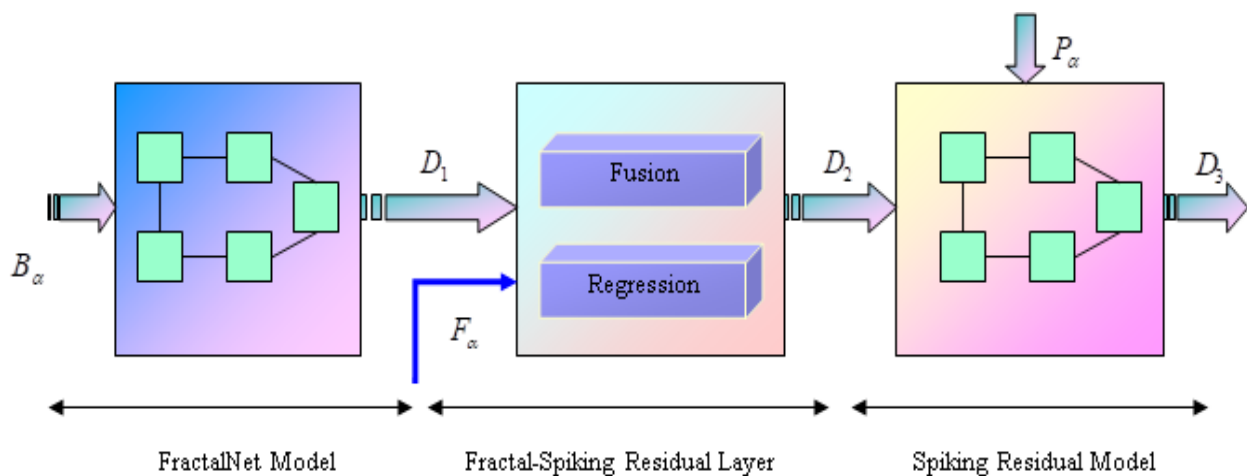


Figure. 3 Systematic view of devised FDSRN

3.6.1. FractalNet model

FractalNet [22] is a deep neural network architecture optimized for classification tasks, integrating convolutional, pooling, and Fully Connected (FC) layers. It begins by passing the input image through a FractalConvNet layer followed by additional pooling and convolutional layers to extract intricate features. These extracted features from both pathways are concatenated and subjected to the FC layer, producing the final classification outcome. This architecture enhances feature representation and classification accuracy in complex datasets. Moreover, FractalNet's integration of concatenated pathways ensures comprehensive feature fusion before final classification. This design not only enhances performance in classification tasks but also supports scalability and adaptability to diverse application domains, making FractalNet a versatile architecture in the realm of deep learning research and applications. The mathematical representation of FractalNet D_1 is given by,

$$D_1 = A(P_\alpha \cdot A_\alpha) \tag{18}$$

Fig. 4 portrays the architecture of the FractalNet model.

3.6.2. Fractal-spiking residual layer

The Fractal-Spiking Residual layer is a specialized component within the FDSRN architecture that integrates fractal-based and spiking neural network principles. It facilitates the fusion of outputs from the FractalNet model and extracted features, enabling advanced regression and fusion processes. The expressions involved in the fractal-spiking residual layer are presented below.

$$M = \sum_{r=1}^z F_\alpha * G_r \tag{19}$$

By applying the Fractional Calculus (FC) concept,

$$K(v + 1) = JK(v) + \frac{1}{2}(v - 1) \tag{20}$$

$$D_2 = J \sum_{r=1}^z F_\alpha * G_r + \frac{1}{2} J D_1 \tag{21}$$

$$D_2 = J \sum_{r=1}^z F_\alpha * G_r + \frac{1}{2} J \cdot A(P_\alpha \cdot A_\alpha) \tag{22}$$

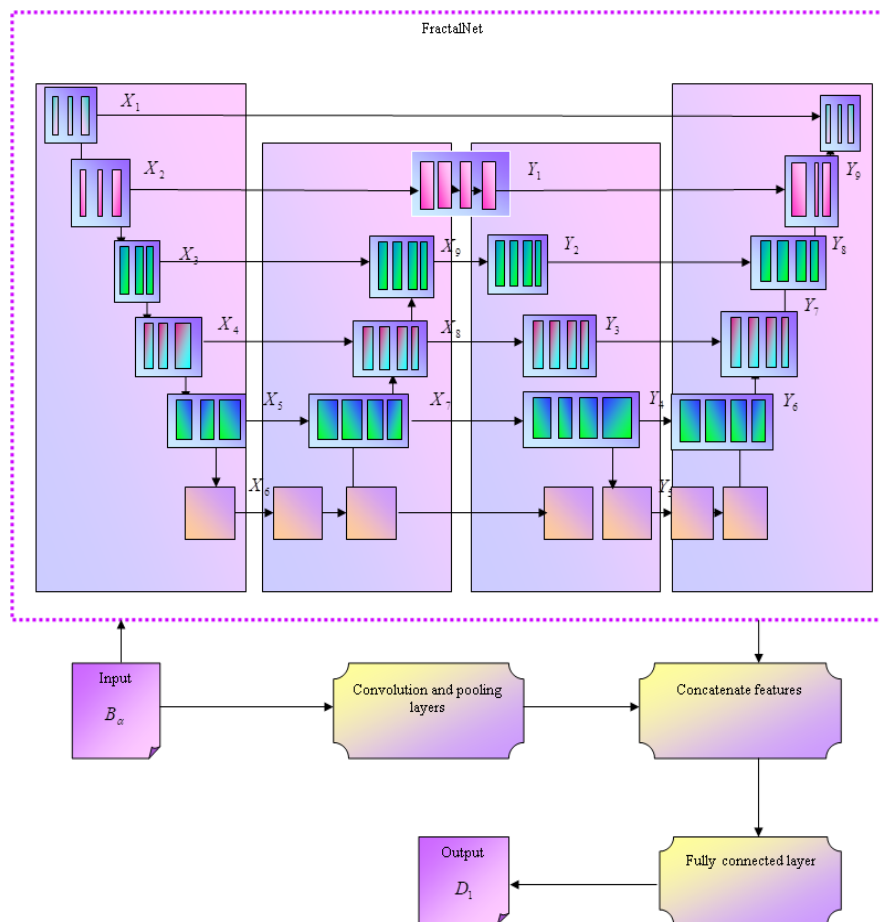


Figure. 4 Architectural diagram of FractalNet model

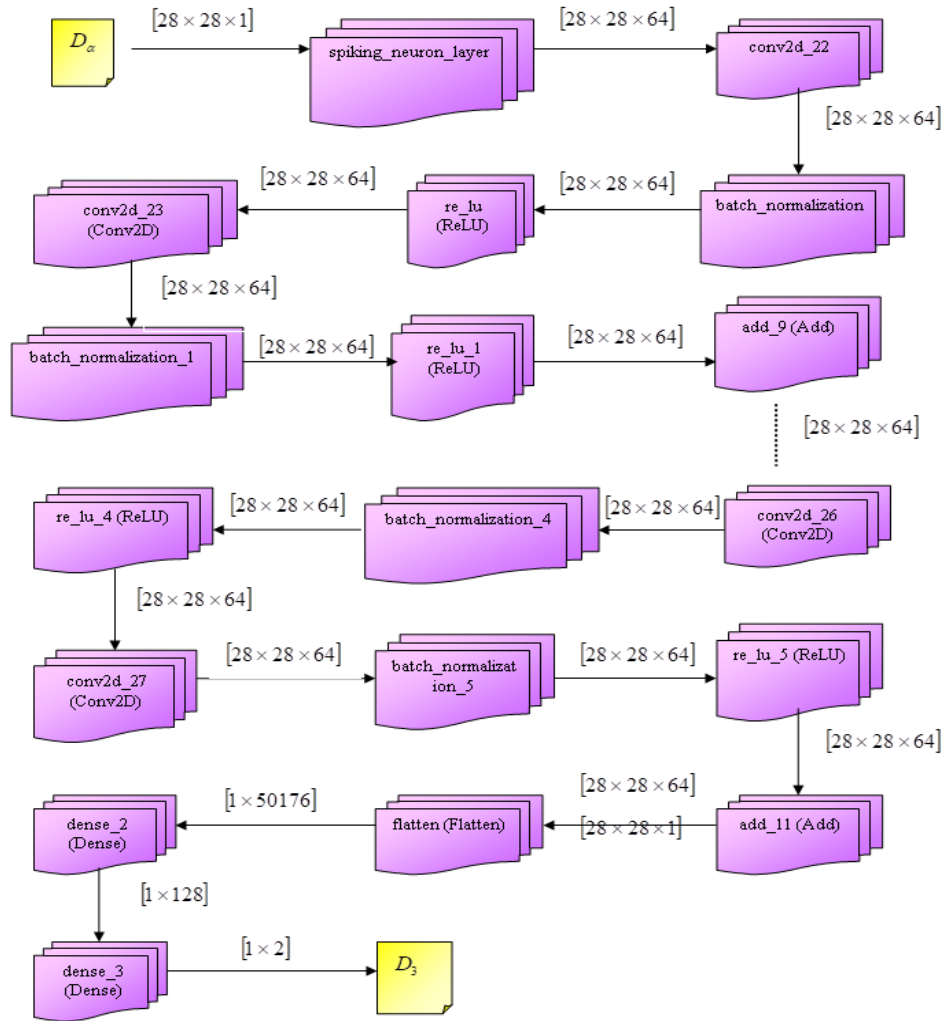


Figure. 5 Structure of spiking residual model

3.6.3. Spiking residual model

The spiking residual model [23] consists of two convolution layers followed by two maximum pooling layers and three FC layers. The Rectified Linear Unit (ReLU) activation functions are used in both FC layers and convolutional layers. The last layer employs the softmax loss function to produce the output of classification. Furthermore, the incorporation of maximum pooling layers after each convolutional block allows the model to downsample feature maps efficiently, capturing salient features while reducing computational complexity. The equation for the spiking residual model is presented below.

$$D_3 = U_2(U_1B + o_1) + o_2 + J \sum_{r=1}^Z F_\alpha * G_r + \frac{1}{2} J \cdot A(P_\alpha \cdot A_\alpha) \quad (23)$$

The structure of the spiking residual model is represented in Fig. 5. In this model, D_α is fed as input

for the spiking residual model, such that $D_\alpha \in \{P_\alpha, D_2\}$.

4. Results and discussion

The outcome discussed by the devised FDSRN for breast cancer identification by employing mammography images is enlisted in this section.

4.1 Experimental setup

Breast cancer detection using the developed FDSRN has been successfully executed with the aid of Python tools.

4.2 Dataset description

The MIAS and Digital Database for Screening Mammography (DDSM) datasets [16] are used for the experimentation.

MIAS dataset (Dataset-1): Here, the original dataset is minimized as 200-micron pixel edge and clipped/padded and the pixel size of each image is 1024×1024 . The database comprises 322 digitized

mammography films, which are stored on a 2.3GB 8mm (ExaByte) tape. Each film includes radiologist annotations, marking the locations of any abnormalities present. This dataset contains 7 columns. The reference number of this dataset is provided in 1st column, the character of the background tissue is given in 2nd column, the abnormality classes are depicted in 3rd column, the severity is given in 4th column, the 5th and 6th columns represent the coordinate centre and the radius is given in column 7.

DDSM dataset (Dataset-2): This database is the result of a collaborative effort between Massachusetts General Hospital, Sandia National Laboratories, and the University of South Florida's Computer Science and Engineering Department. It includes approximately 2,500 studies, each containing two images of each breast along with associated patient information, such as age at the time of the study, ACR breast density rating, subtlety rating for abnormalities, and ACR keyword descriptions of abnormalities. Additionally, it provides image details like scanner type and spatial resolution. For images with suspicious areas, pixel-level “ground truth” data is available, indicating the locations and types of abnormalities. The database also includes software for accessing mammogram and ground truth images, as well as tools for calculating performance metrics for automated image analysis algorithms.

4.3 Performance analysis

The metrics such as accuracy, specificity and sensitivity are employed to evaluate the obtained performance of devised cancer detection model.

4.3.1. Accuracy

Accuracy [28] indicates the overall performance of the devised model while detecting breast cancer. It is mathematically presented as,

$$Accuracy = \frac{W_{\delta} + W_{\omega}}{W_{\delta} + W_{\omega} + V_{\delta} + V_{\omega}} \tag{24}$$

4.3.2. Sensitivity

Sensitivity [28] indicates the ratio of detected cancer cases relative to the total number of actual cancer cases. It can be expressed as,

$$Sensitivity = \frac{W_{\delta}}{W_{\delta} + V_{\omega}} \tag{25}$$

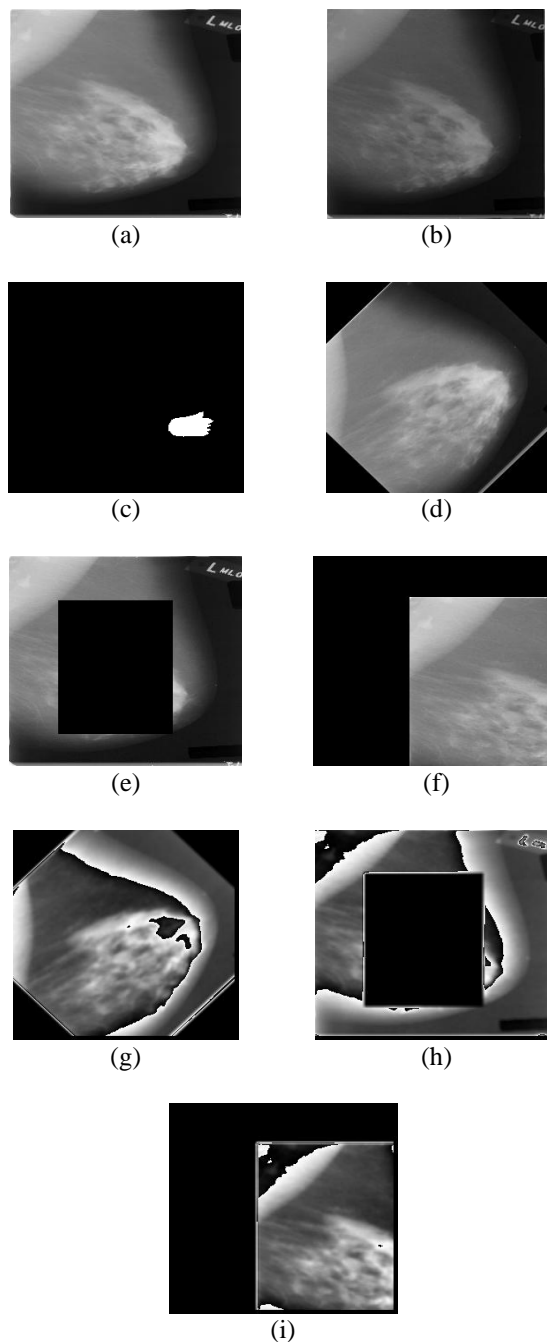


Figure. 6 Experimental result using dataset-1: (a)Input mammogram image, (b)Preprocessed image, (c)Segmented image, (d)Rotated image, (e)Random erased image, (f)Shifted image, (g)Rotated GBP image, (h)Random erased GBP image, and (i)Shifted GBP image

4.3.3. Specificity

Specificity [28] denotes the ratio of detected healthy cases relative to the total number of actual healthy cases. It can be mathematically presented as,

$$Specificity = \frac{W_{\omega}}{W_{\omega} + V_{\delta}} \tag{26}$$

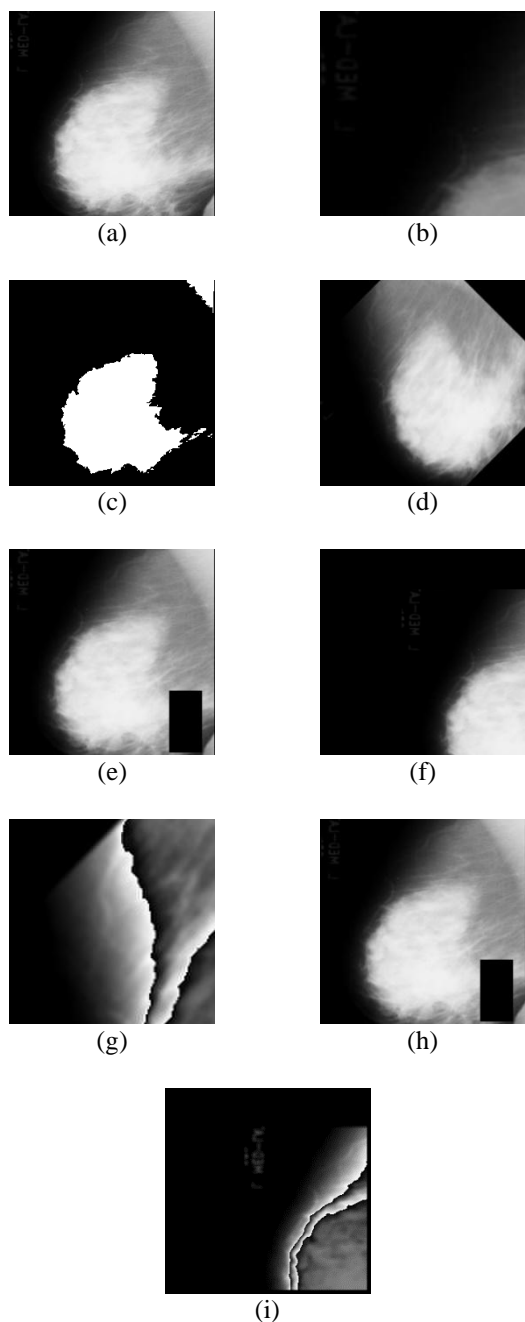


Figure. 7 Experimental result using dataset-2: (a)Input mammogram image, (b)Preprocessed image, (c)Segmented image, (d)Rotated image, (e)Random erased image, (f)Shifted image, (g)Rotated GBP image, (h)Random erased GBP image, and (i)Shifted GBP image

4.4 Experimental result

The experimental findings of the devised FDSRN for breast cancer identification using mammogram images using dataset-1 are displayed in Fig. 6. Fig. 6 a) indicates the mammogram image as input. Fig. 6 b) and Fig. 6 c) illustrate the preprocessed and segmented mammogram image. Fig. 6 d), Fig. 6 e) and Fig. 6 f) present the rotated image, random erased image and shifted image, respectively. Fig. 6 g), Fig.

6 h) and Fig. 6 i) depict the rotated GBP image, random erased GBP image and shifted GBP image, respectively.

Fig. 7 shows the experimental findings of the devised FDSRN using dataset-2. Fig. 7 a) indicates the input mammogram image. Fig. 7 b) and Fig. 7 c) illustrate the preprocessed and segmented mammogram images. Fig. 7 d), Fig. 7 e) and Fig. 7 f) present the rotated image, random erased image and shifted image, respectively. Fig. 7 g), Fig. 7 h) and Fig. 7 i) depict the rotated GBP image, random erased GBP image and shifted GBP image, respectively.

4.6 Comparative methods

The traditional methods, such as SVM [2], ResNet-50 CNN [5], Two-stage DL [12] and Ensemble-Net [14] are used to assess the performance of the introduced FDSRN model.

4.7 Comparative analysis

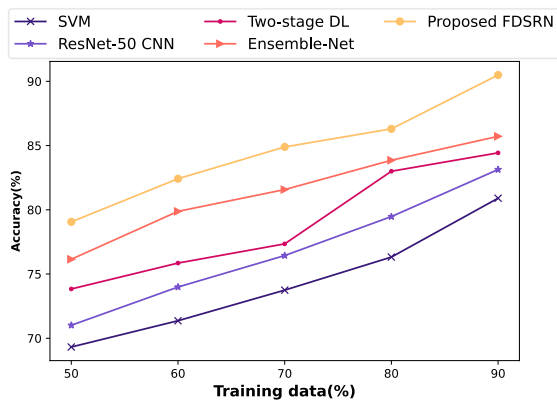
The analysis of the designed FDSRN is accomplished by adjusting both the k-fold value and training data value.

4.7.1. Analysis based on training data for dataset-1

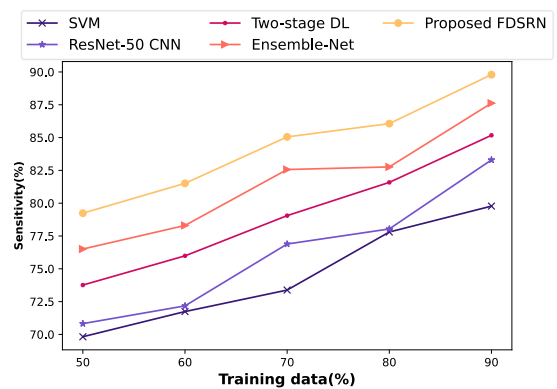
The evaluation of the developed FDSRN is performed by altering training data ranging from 50% to 90% and its assessment in regard to evaluation metrics is illustrated in Fig. 8. Fig. 8 a) represents the performance of the devised FDSRN with accuracy. When training data is chosen as 90%, the devised method achieved an accuracy of 90.490%, while conventional models attained the accuracy of 79.060%, 82.417%, 84.892%, and 86.298%. Fig. 8 b) depicts the performance analysis with regard to sensitivity for training data=90%. The sensitivity values obtained by the prior models and introduced method are 79.238%, 81.512%, 85.051%, 86.063%, and 89.795%. Fig. 8 c) denotes the assessment of the introduced FDSRN scheme based on specificity. Here, the devised method achieved a specificity of 90.901% that shows a performance increment of 12.250% for SVM, 8.717% for ResNet-50 CNN, 7.721% for Two-stage DL, and 3.030% for Ensemble-Net.

4.7.2. Analysis based on k-fold for dataset-1

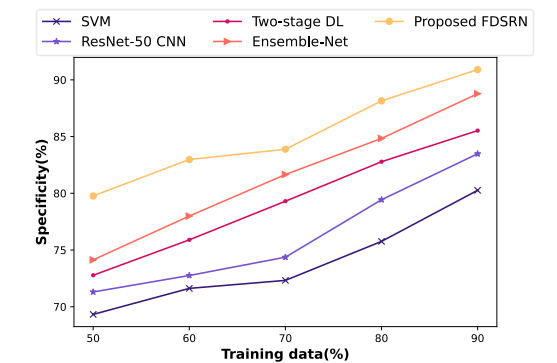
The analysis of the introduced FDSRN is conducted by changing the k-fold value from 5 to 9, is presented in Fig. 9. Fig. 9 a) displays the accuracy performance of the introduced FDSRN. When the k-fold value is selected as 9, the devised FDSRN



(a)



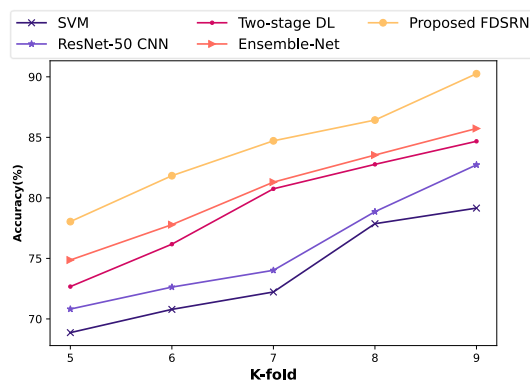
(b)



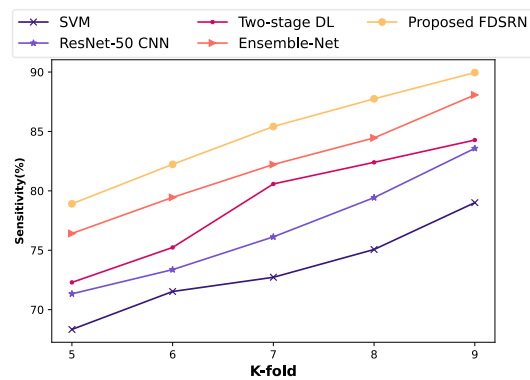
(c)

Figure. 8 Comparative analysis on the basis of training data for dataset-1: (a)Accuracy, (b)Sensitivity, and (c)Specificity

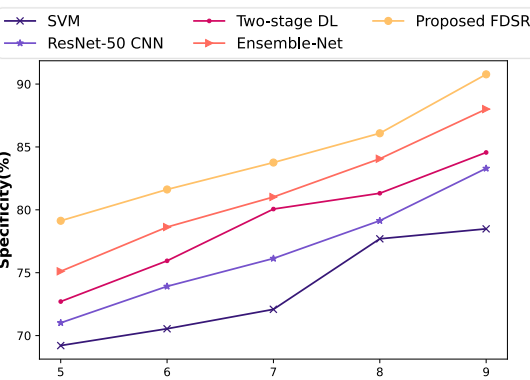
scheme obtained an accuracy rate of 90.255% and the traditional models attained the accuracy as 78.039%, 81.830%, 84.712%, and 86.427% for SVM, ResNet-50 CNN, Two-stage DL and Ensemble-Net, respectively. Fig. 9 b) shows the performance of the devised FDSRN method in accordance with sensitivity. When k-fold=9, the devised model yielded the sensitivity of 89.952% that reveals the performance gain of 12.277%, 8.583%, 5.045%, and 2.455% to that of the conventional techniques. Fig. 9



(a)



(b)



(c)

Figure. 9 Comparative analysis on the basis of k-fold for dataset-1: (a)Accuracy, (b)Sensitivity, and (c)Specificity

c) depicts the assessment of the devised method in terms of specificity. When k-fold value is chosen as 9, the introduced FDSRN method yielded the specificity rate of 90.774% and the prior models gained the specificity as 79.128%, 81.618%, 83.759%, and 86.087%.

4.7.3. Analysis based on training data for dataset-2

The evaluation of the developed FDSRN is carried out by changing the value of training data and K-fold for varying metrics for dataset-2 is depicted in Fig. 10. Fig. 10 a) presents the assessment of the

FDSRN by considering accuracy as an evaluation metric. When the training data is considered as 90%, the traditional model and proposed model achieved accuracy of 79.796%, 81.536%, 83.472%, 85.660%, and 90.144%. This demonstrates the performance gain of 11.479%, 9.548%, 7.401%, and 4.974% over SVM, ResNet-50 CNN, Two-stage DL, and Ensemble-Net, respectively. Fig. 10 b) displays the evaluation of the introduced method using sensitivity. With training data as 90%, the sensitivity achieved by the existing and proposed schemes is 80.477%, 82.783%, 84.592%, 85.224%, and 90.524%. This depicts the performance gain of 11.099%, 8.550%, 6.553%, and 5.855% over other existing techniques.

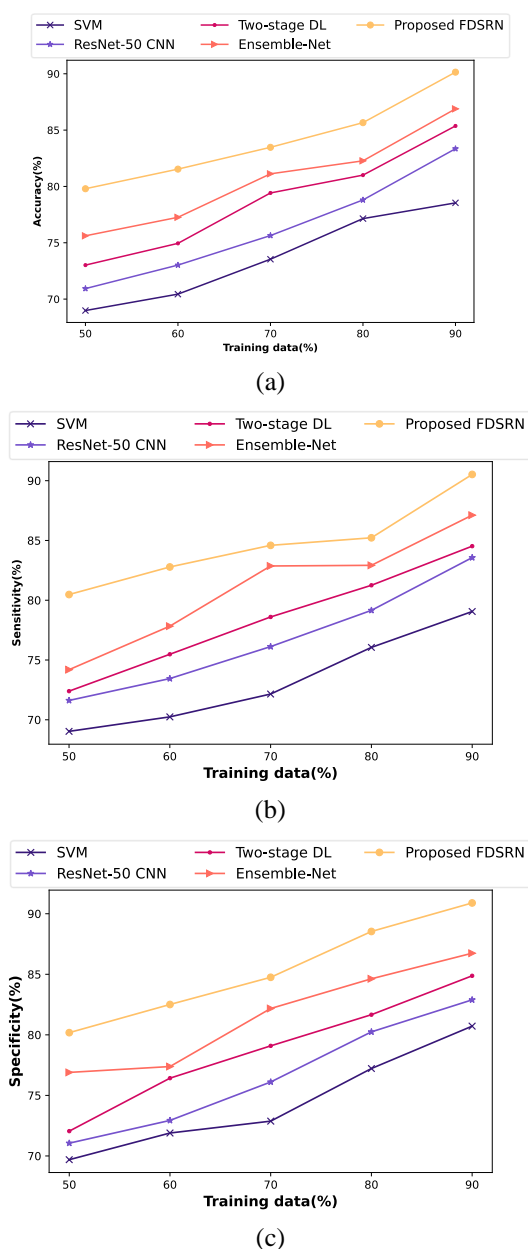


Figure. 10 Comparative analysis on the basis of training data for dataset-2: (a) Accuracy, (b) Sensitivity, and (c) Specificity

Fig. 10 c) presents the assessment of the devised FDSRN method with specificity. With 90% of training data, the existing method and proposed method achieved specificity of 80.181%, 82.507%, 84.752%, 88.536%, and 90.891%. This reveals performance gains of 11.783%, 9.224%, 6.754%, and 2.591% for SVM, ResNet-50 CNN, Two-stage DL, and Ensemble-Net, respectively.

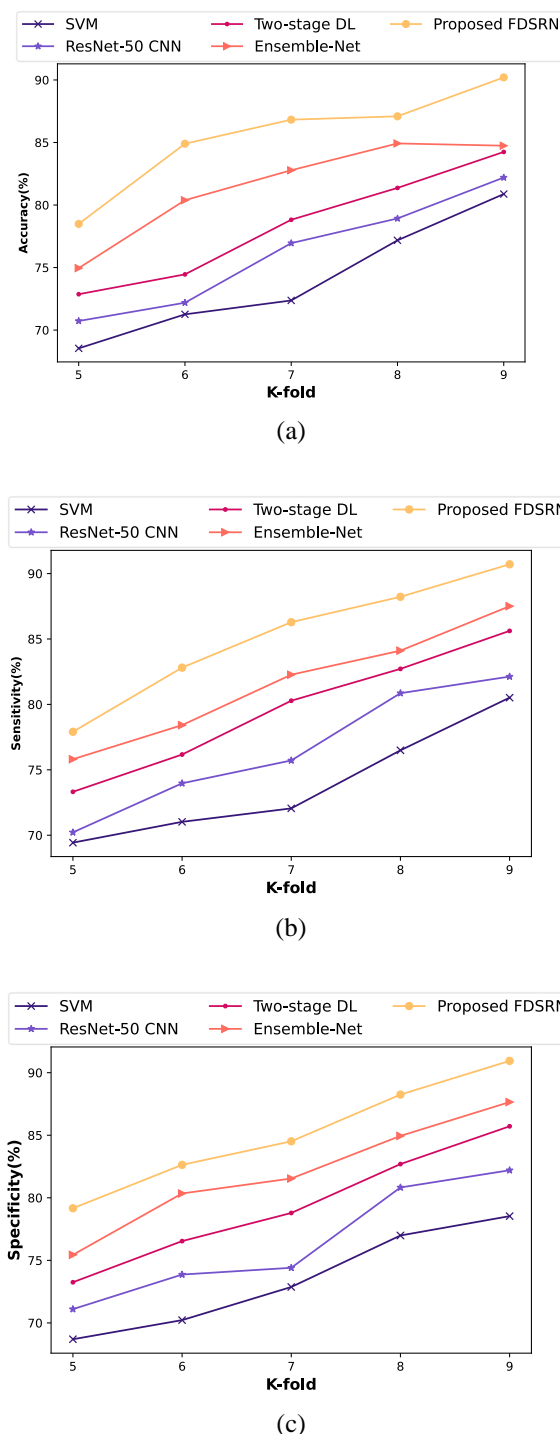


Figure. 11 Comparative analysis on the basis of k-data for dataset-2: (a) Accuracy, (b) Sensitivity, and (c) Specificity

Table 2. Comparative discussion

Variations	Metrics	SVM [2]	ResNet-50 CNN [5]	Two-stage DL [12]	Ensemble-Net [14]	Proposed FDSRN
<i>Dataset-1</i>						
Training data=90%	<i>Accuracy (%)</i>	79.060	82.417	84.892	86.298	90.490
	<i>Sensitivity (%)</i>	79.238	81.512	85.051	86.063	89.795
	<i>Specificity (%)</i>	79.766	82.977	83.882	88.147	90.901
K-fold= 9	<i>Accuracy (%)</i>	78.039	81.830	84.712	86.427	90.255
	<i>Sensitivity (%)</i>	78.908	82.231	85.413	87.744	89.952
	<i>Specificity (%)</i>	79.128	81.618	83.759	86.087	90.774
<i>Dataset-2</i>						
Training data=90%	<i>Accuracy (%)</i>	79.796	81.536	83.472	85.660	90.144
	<i>Sensitivity (%)</i>	80.477	82.783	84.592	85.224	90.524
	<i>Specificity (%)</i>	80.181	82.507	84.752	88.536	90.891
K-fold= 9	<i>Accuracy (%)</i>	78.489	84.902	86.825	87.094	90.205
	<i>Sensitivity (%)</i>	77.906	82.810	86.285	88.224	90.710
	<i>Specificity (%)</i>	79.164	82.633	84.514	88.249	90.943

4.7.4. Analysis based on k-fold for dataset-2

Fig. 11 shows the evaluation of introduced FDSRN by varying the value of k-fold with respect to evaluation metrics. Fig. 11 a) represents the performance of the introduced FDSRN by considering accuracy as evaluation metric. For k-fold value=9, the classical and proposed method achieved accuracy of 78.489%, 84.902%, 86.825%, 87.094%, and 90.205%. This represents performance gain of 12.988%, 5.878%, 3.747%, and 3.449% over SVM, ResNet-50 CNN, Two-stage DL, and Ensemble-Net, respectively. Fig. 11 b) exhibits the performance analysis with regard to the sensitivity. While assuming k-fold value as 9, the devised method attained sensitivity of 90.710%. This indicates the performance evolvment of 14.115%, 8.709%, 4.879%, and 2.741% over SVM, ResNet-50 CNN, Two-stage DL, and Ensemble-Net, respectively. Fig. 11 c) denotes the assessment of the introduced scheme using specificity. The proposed scheme achieved specificity of 90.943% for k-fold=9. This shows the performance gain of 12.952%, 9.138%, 7.069%, and 2.963% over SVM, ResNet-50 CNN, Two-stage DL, and Ensemble-Net, respectively.

4.8 Comparative discussion

Table 2 portrays the discussion conducted by existing models such as SVM, ResNet-50 CNN, Two-stage DL and Ensemble-Net, as well as the proposed FDSRN. The FDSRN method demonstrated better performance compared to classical methods such as SVM, ResNet-50 CNN, Two-stage DL, and Ensemble-Net. Specifically, the devised model achieved impressive scores of 90.490% for accuracy, 89.795% for sensitivity, and 90.901% for specificity when training data=90% for

dataset-1. In contrast, the traditional methods achieved accuracies of 79.060%, 82.417%, 84.892%, and 86.298%, which are lower than those of FDSRN. Thus, the results show the effectiveness of FDSRN which consumes minimum time and complexity while conducting breast cancer detection using mammogram images. Furthermore, while assuming k-fold=9 for dataset-1, the FDSRN system achieved even higher performance with an accuracy of 90.205%, sensitivity of 90.710%, and specificity of 90.943%. This highlights the robustness and superior capabilities of FDSRN over traditional methods by considering accuracy, scalability and detection accuracy.

5. Conclusion

Early detection of breast cancer significantly enhances treatment outcomes by identifying tumors when they are smaller and more localized, thus enabling less invasive and more effective treatment options. This early intervention not only enhances the survival rates but also reduces the need for aggressive therapies like chemotherapy and extensive surgeries, thereby enhancing the overall quality of life for patients. Additionally, early detection allows for the timely implementation of preventive measures and lifestyle changes that can further reduce the risk of cancer recurrence and promote long-term health outcomes. Considering the need for an effective model for breast cancer detection, FDSRN has been devised. Initially, mammogram images undergo preprocessing with a Wiener filter. Next, cancer region segmentation is conducted using U-NeXt. Subsequently, image augmentation techniques like random erasing, rotation and shifting are applied. After augmentation, feature extraction involves extracting BRIEF, GBP, and GLCM. Finally, breast

cancer identification utilizes FDSRN, a hybrid model developed by integrating DSN and FractalNet. The experimental findings of the devised FDSRN shows exceptional performance, with an accuracy of 90.205%, sensitivity of 90.710%, and specificity of 90.943% for dataset-2. In the future, various transfer learning techniques with hybrid optimization can be integrated to enhance severity level of breast cancer.

Conflicts of Interest

The authors declare no conflict of interest.

Author Contributions

Conceptualization, Sachin Urabinahatti; methodology, Sachin Urabinahatti; software, Sachin Urabinahatti; validation, Sachin Urabinahatti, D Jayadevappa, and Mahendra Shivalli Jogigowda; formal analysis, D Jayadevappa; investigation, D Jayadevappa; resources, Mahendra Shivalli Jogigowda; data curation, Mahendra Shivalli Jogigowda; writing—original draft preparation, Sachin Urabinahatti; writing—review and editing, Sachin Urabinahatti; visualization, Sachin Urabinahatti.

References

- [1] E. R. Fearon, "Human cancer syndromes: clues to the origin and nature of cancer", *Science*, Vol. 278, No. 5340, pp.1043-1050, 1997.
- [2] F. A. Al-Fahaidy, B. Al-Fuhaidi, I. AL-Darouby, F. AL-Abady, M. AL-Qadry, and A. AL-Gamal, "A diagnostic model of breast cancer based on digital mammogram images using machine learning techniques", *Applied Computational Intelligence and Soft Computing*, Vol. 1, pp.3895976, 2022.
- [3] R. A. Weinberg, "How cancer arises", *Scientific American*, Vol. 275, No. 3, pp.62-70, 1996.
- [4] J. E. Visvader, "Cells of origin in cancer", *Nature*, Vol. 469, No. 7330, pp.314-322, 2011.
- [5] H. Rahman, T. F. Naik Bukht, R. Ahmad, A. Almadhor, and A. R. Javed, "Efficient breast cancer diagnosis from complex mammographic images using deep convolutional neural network", *Computational intelligence and neuroscience*, Vol. 1, pp.7717712, 2023.
- [6] P. Cowin, T. M. Rowlands, and S. J. Hatsell, "Cadherins and catenins in breast cancer", *Current opinion in cell biology*, Vol. 17, No. 5, pp.499-508, 2005.
- [7] J. R. Benson, I. Jatoti, M. Keisch, F. J. Esteva, A. Makris, and V. C. Jordan, "Early breast cancer", *The Lancet*, Vol. 373, No. 9673, pp.1463-1479, 2009.
- [8] A. S. Elkorany and Z. F. Elsharkawy, "Efficient breast cancer mammograms diagnosis using three deep neural networks and term variance", *Scientific Reports*, Vol. 13, No. 1, pp.2663, 2023.
- [9] H. Avcı and J. Karakaya, "A novel medical image enhancement algorithm for breast cancer detection on mammography images using machine learning", *Diagnostics*, Vol. 13, No. 3, pp.348, 2023.
- [10] K. L. Narayanan, R. S. Krishnan, and Y. H. Robinson, "A Hybrid Deep Learning Based Assist System for Detection and Classification of Breast Cancer from Mammogram Images", *International Arab Journal of Information Technology*, Vol. 19, No. 6, 2022.
- [11] S. S. Chakravarthy, and H. Rajaguru, "Automatic detection and classification of mammograms using improved extreme learning machine with deep learning", *Irbm*, Vol. 43, No. 1, pp.49-61, 2022.
- [12] B. Ibrokhimov, and J.Y. Kang, "Two-stage deep learning method for breast cancer detection using high-resolution mammogram images", *Applied Sciences*, Vol. 12, No. 9, pp.4616, 2022.
- [13] M. Dehghan Rouzi, B. Moshiri, M. Khoshnevisan, M. A. Akhaee, F. Jaryani, S. Salehi Nasab, and M. Lee, "Breast Cancer Detection with an Ensemble of Deep Learning Networks Using a Consensus-Adaptive Weighting Method", *Journal of Imaging*, Vol. 9, No. 11, pp.247, 2023.
- [14] T. Nagalakshmi, "Breast cancer semantic segmentation for accurate breast cancer detection with an ensemble deep neural network", *Neural Processing Letters*, Vol. 54, No. 6, pp.5185-5198, 2022.
- [15] Y. E. Almalki, T. A. Soomro, M. Irfan, S. K. Alduraibi, and A. Ali, "Computerized analysis of mammogram images for early detection of breast cancer", *Healthcare*, Vol. 10, No. 5, pp. 801, 2022.
- [16] The MIAS and DDSM datasets taken from, "<https://www.mammoimage.org/databases>", [Accessed] February, 2024.
- [17] R. Ramani, N. S. Vanitha, and S. Valarmathy, "The pre-processing techniques for breast cancer detection in mammography images", *International Journal of Image, Graphics and Signal Processing*, Vol. 5, No. 5, pp.47, 2013.
- [18] T. Song, F. Meng, A. Rodriguez-Paton, P. Li, P. Zheng, and X. Wang, "U-Next: A novel convolution neural network with an aggregation U-Net architecture for gallstone segmentation in

- CT images”, *IEEE Access*, Vol. 7, pp.166823-166832, 2019.
- [19] M. Calonder, V. Lepetit, M. Ozuysal, T. Trzcinski, C. Strecha, and P. Fua, “BRIEF: Computing a local binary descriptor very fast”, *IEEE Transactions on Pattern Analysis and Machine Intelligence*, Vol. 34, No. 7, pp.1281-1298, 2011.
- [20] K. S. Praveena, “A classical hierarchy method for bone X-ray image classification using SVM”, *International Research Journal of Engineering and Technology (IRJET)*, Vol. 4, No. 8, 2017.
- [21] A. Selvapandian, and K. Manivannan, “Fusion based glioma brain tumor detection and segmentation using ANFIS classification”, *Computer Methods and Programs in Biomedicine*, No. 166, pp.33-38, 2018.
- [22] H. Munusamy, K. J. Muthukumar, S. Gnanaprakasam, T. R. Shanmugakani, and A. Sekar, “FractalCovNet architecture for COVID-19 chest X-ray image classification and CT-scan image segmentation”, *Biocybernetics and Biomedical Engineering*, Vol. 41, No. 3, pp.1025-1038, 2021.
- [23] Y. Hu, H. Tang, and Pan, G., “Spiking deep residual networks”, *IEEE Transactions on Neural Networks and Learning Systems*, Vol. 34, No. 8, pp.5200-5205, 2021.
- [24] N. E. Khalifa, M. Loey, and S. Mirjalili, “A comprehensive survey of recent trends in deep learning for digital images augmentation”, *Artificial Intelligence Review*, Vol. 55, No. 3, pp.2351-2377, 2022.
- [25] P. M. Bhate, and S. B. Patil, “Data Mining Techniques for Customer Relationship Management in Organized Retail Industry”, In: *Proc. of National Conference*, pp. 35.
- [26] S. S. Sinare and P. S. Vikhe, “Fuzzy C-means Clustering Algorithm for Breast Cancer Detection”, *International Journal of Advanced and Innovative Research*, pp.307, 2012.
- [27] L. R. Chilakala and G.N. Kishore, “Optimal deep belief network with opposition-based hybrid grasshopper and honeybee optimization algorithm for lung cancer classification: A DBNGHHB approach”, *International Journal of Imaging Systems and Technology*, Vol. 31, No. 3, pp.1404-1423, 2021.
- [28] Y. Muhammad, M. Tahir, M. Hayat, and K. T. Chong, “Early and accurate detection and diagnosis of heart disease using intelligent computational model”, *Scientific reports*, Vol. 10, No. 1, pp.19747, 2020.